



Gamma/Hadron Separation Method for the HADAR Experiment

Yang-Zhao Ren¹, Tian-Lu Chen¹, You-Liang Feng¹, Dan-Zeng Luo-Bu¹, Yi-Qing Guo^{2,3}, Cheng Liu², Qi Gao¹, Mao-Yuan Liu¹, Xiang-Li Qian⁴, Ya-Ping Wang¹, Zi-Hao Zhang¹, Xin-Long Li¹, Qing-Yuan Hou¹, Heng-Jiao Liu¹, Qing-Qian Zhou¹, and Shan-Jie Shu¹

¹ The Key Laboratory of Cosmic Rays (Tibet University), Ministry of Education, Lhasa 850000, China; chentl@ihep.ac.cn, fengyouliang@utibet.edu.cn

² Key Laboratory of Particle Astrophysics, Institute of High Energy Physics, Chinese Academy of Sciences, Beijing 100049, China

³ University of Chinese Academy of Sciences, Beijing 100049, China

⁴ School of Intelligent Engineering, Shandong Management University, Jinan 250357, China

Received 2023 October 30; revised 2024 January 10; accepted 2024 January 27; published 2024 February 20

Abstract

Ground-based arrays of imaging atmospheric Cherenkov telescopes (IACTs) are the most sensitive γ -ray detectors for energies of approximately 100 GeV and above. One such IACT is the High Altitude Detection of Astronomical Radiation (HADAR) experiment, which uses a large aperture refractive water lens system to capture atmospheric Cherenkov photons (i.e., the imaging atmospheric Cherenkov technique). The telescope array has a low threshold energy and large field of view, and can continuously scan the area of the sky being observed, which is conducive to monitoring and promptly responding to transient phenomena. The process of γ -hadron separation is essential in very-high-energy (>30 GeV) γ -ray astronomy and is a key factor for the successful utilization of IACTs. In this study, Monte Carlo simulations were carried out to model the response of cosmic rays within the HADAR detectors. By analyzing the Hillas parameters and the distance between the event core and the telescope, the distinction between air showers initiated by γ -rays and those initiated by cosmic rays was determined. Additionally, a Quality Factor was introduced to assess the telescope's ability to suppress the background and to provide a more effective characterization of its performance.

Key words: astroparticle physics – telescopes – methods: data analysis

1. Introduction

The Vela satellites first detected γ -ray bursts (GRBs) in the late 1960s. Since then, GRBs have garnered extensive interest owing to their extreme brightnesses, cosmological distances and potential connections with massive stellar collapses and compact binary coalescence events (Kumar & Zhang 2015). In recent years, γ -ray source detection capabilities have substantially improved, resulting in the discovery of over 200 very-high-energy (VHE) γ -ray sources (Ajello et al. 2019). The majority of these VHE γ -ray sources were observed through imaging atmospheric Cherenkov telescopes (IACTs), such as the High Energy Stereoscopic System (Benbow & HESS Collaboration 2005), Very Energetic Radiation Imaging Telescope Array System (Park 2015) and Major Atmospheric Gamma Imaging Cherenkov Telescopes (Ahnen et al. 2017). However, their small fields of view and low duty cycles rendered them unsuitable for extensive monitoring activities and promptly responding to transients. To address this issue, the High Altitude Detection of Astronomical Radiation (HADAR) experiment, a ground-based experimental array with a low energy threshold and wide field of view, was proposed. As VHE γ -rays penetrate the atmosphere, they interact with atomic nuclei (primarily oxygen and nitrogen) (Yao 2006), generating secondary particles. As these particles

exceed the local phase velocity of light in the medium of the air (Chen et al. 2019), they produce Cherenkov light. The HADAR experiment employs a distinct optical system to collect photon data, which are used to reconstruct primary γ -ray events. Given that the share of γ -ray initiated showers is dwarfed by the proton-initiated events, Cherenkov light similar to γ -ray showers produced by protons must serve as the primary background signal in the practical observation of GRBs (Andringa et al. 2007). The process of γ -hadron segregation enables γ signals to be distinguished from a strong cosmic-ray background, which enhances the accuracy of γ -ray energy spectrum measurements and further reveals information on the origin, acceleration, and propagation of high-energy particles in the universe (Adams et al. 2022) and the nature of non-thermal processes that generate GRBs (Klebesadel et al. 1973). Furthermore, γ -hadron separation techniques provide crucial supplemental data for multi-band (e.g., X-ray, ultraviolet and radio) and multi-messenger research (Flinders 2015).

The rest of this paper is organized as follows. Section 2 gives an overview of the HADAR experiment. In Section 3, we explain the software we developed for event reconstruction and analysis of atmospheric Cherenkov telescope data. Section 4 discusses the result of the study, and Section 5 contains the summary and conclusions.

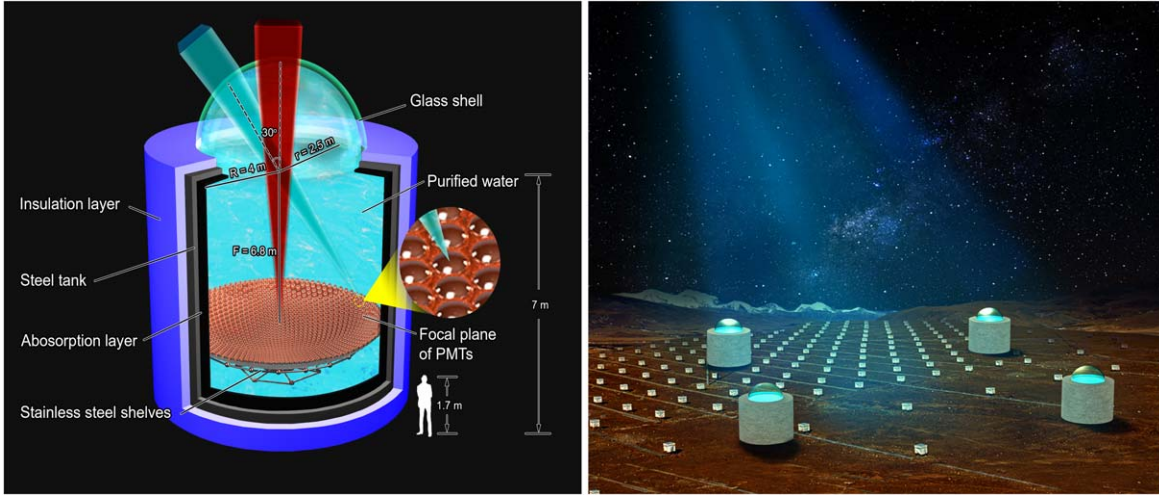


Figure 1. Schematic of HADAR experiment. Left: sectional view of a single water-lens. Right: overall layout of the HADAR experimental observation array (adopted from Xin et al. 2021).

2. Experiment

Based on Gamma Air Watch (Cusumano et al. 2011) and the Fresnel lens telescope in the Joint Experiment Module for the Extreme Universe Space Observatory (Casolino et al. 2011), the HADAR experiment is a super wide-angle atmospheric Cherenkov telescope array comprised of four large-aperture, wide-angle water lenses that mimic the structure of the human eye. Figure 1(left) displays a detailed schematic of a single water lens (Xin et al. 2021), which consists of a 5 m diameter hemispherical acrylic shell mounted on an 8 m diameter steel tank. The tank consists of, from the outermost layer inwards, an insulation layer (for maintaining a consistent tank temperature), a steel frame (for providing internal structural support) and an absorption layer (which prevents multiple reflections of photons within the tank). The tank is filled with ultra-pure water to maximize the transmittance of ultraviolet photons. The imaging system (referred to here as the camera) of this lens is comprised of 18,961 2 inch photomultiplier tubes (PMTs) (Qian et al. 2022) positioned on the focal plane of the lens. Each water lens is designed to focus parallel light incident on its edge onto the edge of the camera, thereby extending the field of view of a single water lens to 60° . The PMTs are supported by a steel structure beneath them. The overall layout of the HADAR experiment is illustrated in Figure 1(right) (adopted from Xin et al. 2021). The four water lenses are positioned at the vertices of a square with a side length of 100 m. In the figure, the small white squares indicate the scintillation detector array (SA) of the YangBaJing Hybrid array (Feng et al. 2019), which can be used for future joint observations. On clear, moonless nights, Cherenkov photons generated by γ -ray-initiated air showers are collected and refracted by the water lens, with the beam converging on the

camera of the water lens to enable the Cherenkov light to be imaged. Combining the stereo imaging capability of the four telescopes with Hillas parameter modeling enhances our ability to differentiate γ -ray events from cosmic-ray proton events.

3. Simulation

To maximize the observational capabilities of the HADAR experiment, we developed software specifically for event reconstruction and analysis of atmospheric Cherenkov telescope data. The simulation specifications were as follows. Atmospheric Cherenkov light originating from Extensive Air Showers was simulated using the COsmic Ray SIMulations for KAscade (CORSIKA) software package (Version 74100), with the atmospheric Cherenkov mode selected. For the high- and low-energy hadronic interaction models, we used QGSJETII-04 (Ostapchenko 2006) and FLUKA (MacKinnon et al. 2020), respectively. The simulation was performed at an altitude of 4300 m, which corresponded to an atmospheric depth of 606 g cm^{-2} . The geomagnetic coordinates were set to correspond to Yangbajing in Tibet ($30^\circ 08' 48'' \text{N}$, $90^\circ 55' 22'' \text{E}$). The initially simulated γ -rays had energies ranging from 50 GeV to 10 TeV, and the energies of the initial protons ranged from 50 GeV to 30 TeV. A typical power law energy spectrum with a spectral index of 2.7 was adopted for the primary particles. Within this energy range, 4.10×10^6 γ -ray-induced air shower events and 4.30×10^6 proton-induced air shower events were generated. The zenith angle of the initial particle incidence was 0° – 30° and the azimuth range spanned from 0° to 360° . To ensure the creation of a sufficiently large sampling area that contained nearly all events that could trigger the array, all air showers were generated in a uniformly distributed circular area

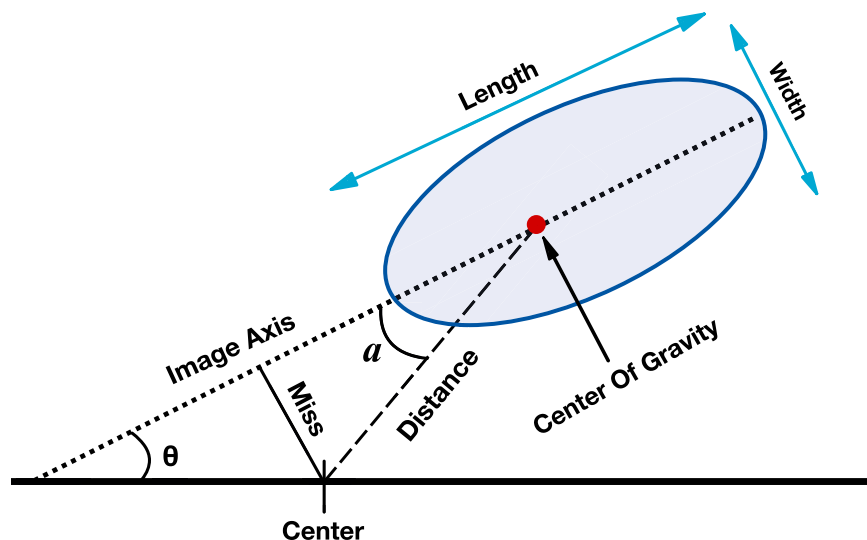


Figure 2. Definitions of the Hillas parameters.

that was centered on the middle of the array and that had a radius of approximately 350 m.

In the simulation phase, the camera was assigned the following trigger algorithm: if the number of photons gathered by a single PMT within a time window of 20 ns was ≥ 9 , it was considered to have been triggered; if the number of adjacent PMTs triggered was ≥ 3 , the telescope was considered to have been triggered; and if the number of telescopes triggered was ≥ 2 , the array was deemed to have been triggered (Xin et al. 2022). For high-energy events, the single PMT trigger threshold was higher (Colin et al. 2009). If the number of photons collected by a single PMT for a cosmic-ray event exceeded the assigned threshold, that PMT was recorded as a pixel, and the total set of logged pixels composed the Cherenkov light image. The Cherenkov photon images generated by each telescope were independently calibrated, extracted and parameterized. As the longitudinal spread of air showers induced by γ -rays is large and their lateral spread is small (Hillas 1985), they appear as an ellipse in an image. To describe this ellipse and its orientation parameters within the imaging system, the Hillas parameters were used (Weekes et al. 1989). These parameters, which are displayed in Figure 2 and listed below, constitute the basic prerequisites for performing γ -hadron separation. The shapes of such ellipses are usually described by the first- and second-order moments of the image intensity distribution; the first-order moment indicates the Center Of Gravity (COG) of the ellipse and the second-order moment describes the lengths of the major and minor axes of the ellipse (Aharonian et al. 2006). This information is instrumental for subsequent analysis and event reconstruction.

1. Size: the total light content of the image (in digital counts), calculated by summing the charge of all the pixels in an image
2. Center of gravity (COG): the COG of the distribution of the photons in an image
3. Length: the root mean square (rms) spread of the light along the major axis of the ellipse; represents the longitudinal spread of the shower
4. Width: the rms spread of the light along the minor axis of the ellipse; represents the lateral spread of the shower
5. Alpha: the angle between the major axis of the ellipse and the line joining the COG to the camera's center
6. Distance: the distance from the center of the camera to the COG of the image.

4. Methods and Results

As electromagnetic cascades are typically focused, the majority of γ -ray events can be imaged as ellipses with high-eccentricity ratios. As a result of the leading particle effect and the directional randomness of hadron cascades, cosmic-ray proton events produce scattered and irregular images (Das & Boruah 2023). Additionally, parameters such as the zenith angle of the event, distance from the event core to the telescope and energy of the event affect the shape of the shower image. To distinguish between air showers initiated by γ -rays from those initiated by hadrons, we performed γ -hadron separation via Monte Carlo (MC) simulations. First, a lookup table was established based on the impact parameters, which include the distance from the event's core to each telescope (hereinafter referred to as D_r) and the Hillas parameters. As mentioned

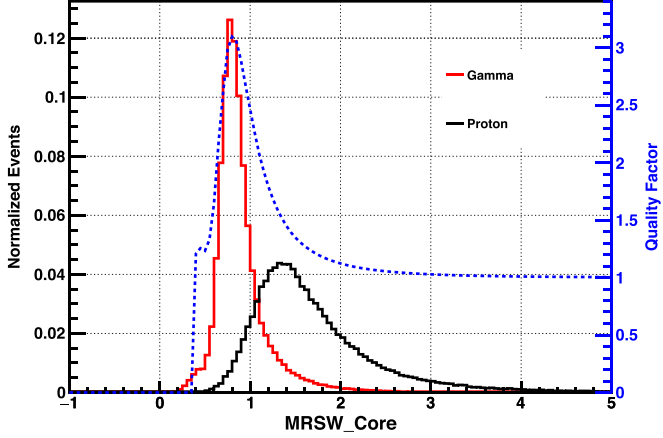


Figure 3. The panel demonstrates the distribution of the normalized MRSW_Core parameter for photon-initiated (red line) and proton-initiated (black line) events. The y-axis coordinates on the right correspond to the Q Factor, which is shown as the blue dotted line in the figure.

earlier, during the simulation all events were projected within a circle with a radius of 350 m centered on the HADAR array. To include as many events as possible, the maximum and minimum Dr (Dr_{\max} and Dr_{\min} , respectively) were set to 500 and 0 m, respectively. The distance from Dr_{\max} to Dr_{\min} was divided into 20 bins, each spanning 25 m. Based on the Hillas parameters, we calculated the total number of events in each bin along with the $Width$ of each event (which was derived from the fitted ellipse). For each bin, the sum of the $Width$ values of all events was then divided by the total number of events to obtain the average $Width$ (Ave_W) of the events. These measurements were used to establish the lookup table. Next, air showers caused by γ -rays and those caused by protons were differentiated by calculating the Mean Reduced Scaled Width (MRSW_Core), which is expressed as

$$MRSW_Core = \frac{1}{N_{tri}} \left(\frac{Width_i}{Ave_W[20]} \right), \quad (1)$$

where $Width_i$ denotes the width value of the image formed by the i_{th} ($i = 1, 2, 3, 4$) telescope detecting the event, $Ave_W[20]$ signifies the 20-element array that is extracted from the lookup table and N_{tri} is the number of telescopes triggered. The Dr range of an event can be determined using the software employed in this study.

Figure 3 shows the γ -hadron distribution calculated via the MRSW_Core method. The γ event image in the figure is centered at approximately $MRSW_Core = 0.8$ and is relatively narrow, while the proton event image is broader. These observations suggest that the MRSW_Core can serve as an effective parameter for filtering and suppressing background events. The Quality Factor's (Q Factor's) magnitude signifies the efficiency of background suppression (Krause et al. 2017) and is represented by the blue dotted line in the figure. It is

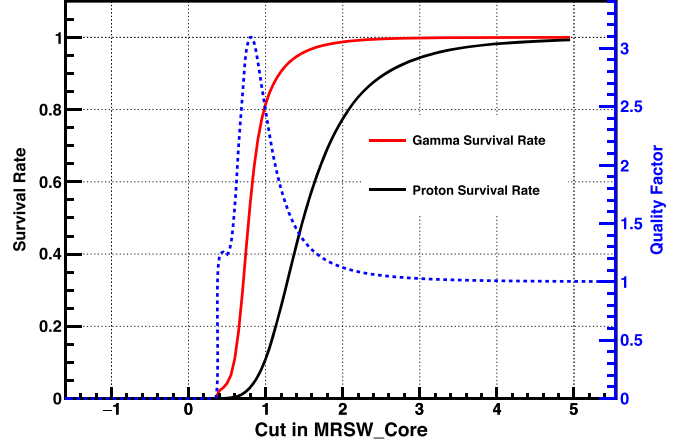


Figure 4. Survival rates of the γ -rays and protons corresponding to Figure 3. The red and black lines represent γ -rays and protons, respectively. The y-axis coordinates on the left indicate the survival rates of both; the coordinates on the right indicate the Q Factor, which are shown as the blue dotted line. The maximum value of the Q Factor, 3.09, is achieved at 0.8.

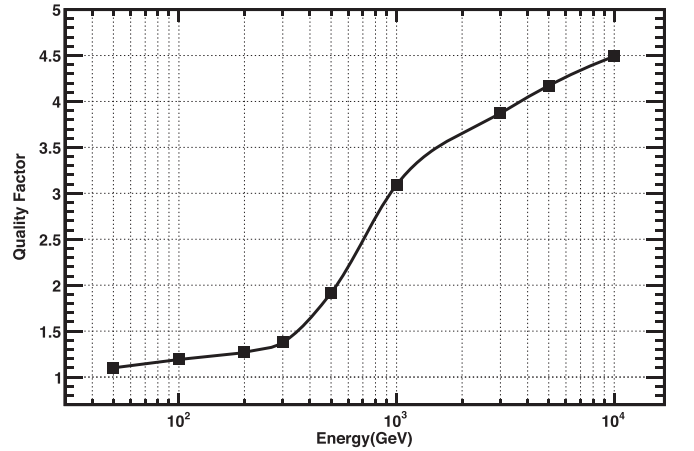


Figure 5. Relationship between the Q Factor and energy.

calculated as

$$Q = \frac{\epsilon_\gamma}{\sqrt{\epsilon_p}}, \quad (2)$$

where ϵ_γ is the ratio of the simulated γ -rays found after identification to the simulated γ -rays generated before identification (i.e., the survival rate of γ -rays) and ϵ_p is the ratio of the simulated protons found after identification of the simulated protons generated before identification (i.e., the survival rate of protons). As illustrated in Figure 4, which displays the survival rates of the γ -rays and protons corresponding to Figure 3, the Q Factor reaches its maximum value when Cut in MRSW_Core = 0.8, yielding survival rates for γ -rays and protons of 54.03% and 3.06%, respectively.

The results in Figure 5 display the Q Factor values at varying energy levels and were obtained using the MRSW_Core as a filtering parameter. Within the low-energy section, discerning between γ -ray and proton events poses a challenge because, under such conditions, the Cherenkov light generated by a shower is sparse and an even smaller number of photons reaches the observation plane, resulting in insufficient data to produce distinguishable images.

5. Summary

Although the study of GRB afterglow radiation models has reached a certain level of maturity, instantaneous radiation theory still requires additional experimental data for further substantiation (Waxman 1995). The HADAR experiment provides an effective solution for ground-based detection of instantaneous radiation from GRBs. Its broad field of view covers a larger region on the sky than most arrays, potentially filling the existing gap in instantaneous GRB radiation detection. In this study, the process of γ -hadron discrimination played an essential role, resulting in the successful differentiation of γ -rays and cosmic protons in synthesized HADAR experimental data obtained using MC simulations. The results validate both the feasibility and efficacy of the proposed method for γ -hadron separation. Future plans involve implementing this method in the HADAR experiment to enhance our understanding and analysis of experimental data.

Acknowledgments

This work was supported by the Central Government Funds for Local Scientific and Technological Development

(grant No. JDRC2023000009), and Tibet University Post-graduate Students' High-Level Talent Training Plan Project (grant No. 2021-GSP-S038).

References

- Adams, C. B., Benbow, W., Brill, A., et al. 2022, *A&A*, **658**, A83
 Aharonian, F., Akhperjanian, A. G., Bazer-Bachi, A. R., et al. 2006, *A&A*, **457**, 899
 Ahnen, M. L., Ansoldi, S., Antonelli, L. A., et al. 2017, *Aph*, **94**, 29
 Ajello, M., Arimoto, M., Axelsson, M., et al. 2019, *ApJ*, **878**, 52
 Andringa, S., Assis, P., Pimenta, M., et al. 2007, arXiv:0707.4467
 Benbow, W. & HESS Collaboration 2005, in AIP Conf. Proc. 745 (New York: AIP), 611
 Casolino, M., Adams, J. H., Bertaina, M. E., et al. 2011, *ASTRA*, **7**, 477
 Chen, T. L., Liu, C., Gao, Q., et al. 2019, *NIMPR*, 927, 46
 Colin, P., Tridon, D. B., Carmona, E., et al. 2009, arXiv:0907.0960
 Cusumano, G., Agnetta, G., Arruda, L., et al. 2011, in Proc. 32nd ICRC, 9 (Beijing: ICRC), 260
 Das, P. R., & Boruah, K. 2023, *InJPh*, **97**, 347
 Feng, Y. L., Zhang, Y., Chen, T. L., et al. 2019, *ChPhC*, **43**, 075002
 Flinders, A. 2015, arXiv:1509.04224
 Hillas, A. M. 1985, in Proc. 19th ICRC, 3 (Beijing: ICRC), 445
 Klebesadel, R. W., Strong, I. B., & Olson, R. A. 1973, *ApJL*, **182**, L85
 Krause, M., Pueschel, E., & Maier, G. 2017, *Aph*, **89**, 1
 Kumar, P., & Zhang, B. 2015, *PhR*, **561**, 1
 MacKinnon, A., Szpigel, S., Gimenez de Castro, G., et al. 2020, *SoPh*, **295**, 174
 Ostapchenko, S. 2006, *NuPhS*, **151**, 143
 Park, N. 2015, arXiv:1508.07070
 Qian, X. L., Sun, H. Y., Chen, T. L., et al. 2022, *FrPhy*, **17**, 64602
 Waxman, E. 1995, *PhRvL*, **75**, 386
 Weekes, T. C., Cawley, M. F., Fegan, D. J., et al. 1989, *ApJ*, **342**, 379
 Xin, G. G., Cai, H., Guo, Y. Q., et al. 2022, *Nucl. Sci. Tech.*, **33**, 25
 Xin, G. G., Yao, Y. H., Qian, X. L., et al. 2021, *ApJ*, **923**, 112
 Yao, W. M. 2006, *JPhG*, **33**, 1